Energetics of intrinsic defects and their complexes in ZnO investigated by density functional calculations

R. Vidya,[1,*] P. Ravindran,[1] H. Fjellvåg,[1] B. G. Svensson,[2] E. Monakhov,[2] M. Ganchenkova,[3] and R. M. Nieminen[3]

[1]*Center for Materials Science and Nanotechnology and Department of Chemistry, University of Oslo, Box 1033 Blindern, N-0315 Oslo, Norway*

[2]*Center for Materials Science and Nanotechnology and Department of Physics, Physical Electronics, University of Oslo, Box 1048 Blindern, N-0316 Oslo, Norway*

[3]*Laboratory of Physics, Helsinki University of Technology, P.O. Box 1100, F-02015 HUT, Finland*

(Received 21 June 2010; revised manuscript received 29 September 2010; published 31 January 2011)

Formation energies of various intrinsic defects and defect complexes in ZnO have been calculated using a density-functional-theory-based pseudopotential all-electron method. The various defects considered are oxygen vacancy (V_O), zinc vacancy (V_{Zn}), oxygen at an interstitial site (O_i), Zn at an interstitial site (Zn_i), Zn at V_O (Zn_O), O at V_{Zn}(O_{Zn}), and an antisite pair (combination of the preceding two defects). In addition, defect complexes like ($V_O + Zn_i$) and Zn-vacancy clusters are studied. The Schokkty pair ($V_O + V_{Zn}$) and Frenkel pairs [($V_O + O_i$) and ($V_{Zn} + Zn_i$)] are considered theoretically for the first time. Upon comparing the formation energies of these defects, we find that V_O would be the dominant intrinsic defect under both Zn-rich and O-rich conditions and it is a deep double donor. Both Zn_O and Zn_i are found to be shallow donors. The low formation energy of donor-type intrinsic defects could lead to difficulty in achieving *p*-type conductivity in ZnO. Defect complexes have charge transitions deep inside the band gap. The red, yellow, and green photoluminescence peaks of undoped samples can be assigned to some of the defect complexes considered. It is believed that the red luminescence originates from an electronic transition in V_O, but we find that it can originate from the antisite Zn_O defect. Charge density and electron-localization function analyses have been used to understand the effect of these defects on the ZnO lattice. The electronic structure of ZnO with intrinsic defects has been studied using density-of-states and electronic band structure plots. The acceptor levels introduced by V_{Zn} are relatively localized, making it difficult to achieve *p*-type conductivity with sufficient hole mobility.

DOI: 10.1103/PhysRevB.83.045206 PACS number(s): 71.15.Nc, 81.05.Je, 71.20.−b

I. INTRODUCTION

Transparent conducting oxides are utilized for a wide range of applications, such as electrodes in thin film transistor, liquid crystal display[1] or the window layers for thin-film solar cells.[2] Although indium tin oxide is currently used in manufacturing, research for an immediate alternative to indium tin oxide is desirable because of the high cost and scarcity of indium. In recent years, zinc oxide (ZnO) has attracted more attention because the Zn element is relatively cheap and abundant.

ZnO is a high-efficiency, low-voltage phosphor in the green range for vacuum fluorescent displays and field emission displays.[3] ZnO also attracts great attention due to its promising applications as ultraviolet light-emitting diodes, laser diodes,[4] and transparent thin-film transistors.[5] A basic understanding of the physical properties of ZnO is required for its use in technological applications. It is well known that properties of materials greatly depend on the defects present. It is widely accepted that defect luminescence in ZnO falls into three main bands in ZnO: a green luminescence (GL) band around 510 nm (2.431 eV), a yellow luminescence (YL) band around 570 nm (2.175 eV), and a red/orange luminescence band at 650 nm (1.907 eV).

Even though ZnO has received a lot of attention in recent years, experimental studies are inconclusive in pointing out the predominant defect type and the physical mechanisms behind the visible luminescence are still under controversy. For example, despite the many experimental observations of GL, its origin is still not understood. In general, two possible mechanisms for the green emission are considered: (i) recombination of a shallowly trapped electron with a deeply trapped hole and (ii) recombination of a shallowly trapped hole with a deeply trapped electron. Due to the low formation energy, oxygen vacancies are abundant as donors and proposed to be the origin of GL in undoped ZnO. The 560-nm (2.214-eV) emission peak is attributed to the electron transition from the conduction band to the doubly ionized oxygen-vacancy defects (V_O^{2+}) located 2.2 eV below the conduction-band edge.[6] Chichibu *et al.*[7] argued that certain point defect complexes associated with a zinc vacancy (V_{Zn}) are the dominant nonradiative centers. These defect complexes can lead to reductions of the band edge emission that are observed in both undoped and doped ZnO, and their origin is still an open question. Moreover, investigations on visible emissions are further complicated, as ZnO samples prepared by different techniques[8] exhibit different characteristics.

In calculations one has the possibility to simulate systems without any defects as well as systems doped with desired impurities. Further theory has the additional degree of freedom that one can isolate various defects and defect complexes and study their stability and their role in optoelectronic properties. Extensive theoretical treatment of intrinsic defects has been carried out.[9–22] Especially, the role of oxygen vacancy in *n*-type conductivity of ZnO has been under intense focus. Calculation of the formation energy of different intrinsic defects was first done by Kohan *et al.*,[9] who showed that V_O is indeed a negative-*U* defect and has the lowest formation energy under Zn-rich conditions. As the band gap of ZnO is underestimated by density functional calculations, many

different correction schemes have been adapted by different authors. By correcting the local density approximation (LDA) band-gap error using an extrapolation scheme using the LDA + U method, Janotti and Van de Walle[18] have shown that V_O is a deep donor, with the (2+/0) transition occurring at 1.0 eV below the conduction-band minimum (CBM). Paudel *et al.*[20] used an LDA + U_d + U_s scheme, whereas recent calculations[21,22] based on hydrid functionals have reproduced the experimental band gap of ZnO and shown that V_O is indeed a deep double donor.

Even though many theoretical studies are made on elementary point defects, studies on defect complexes are hitherto not available. Therefore, we have attempted to explore different types of defect complexes for the first time, employing density-functional calculations. The following point defects are considered: (1) oxygen vacancy (V_O), (2) zinc vacancy (V_{Zn}), (3) oxygen at an interstitial site (O_i), (4) interstitial Zn (Zn_i), (5) antisite defect-like Zn at an oxygen site (Zn_O), (6) oxygen at a Zn site (O_{Zn}), and an antisite pair (pair; $Zn_O + O_{Zn}$ complex). In addition, defect complexes like Frenkel pairs (1) V_O and O_i ($V_O + O_i$) and (2) V_{Zn} and Zn_i ($V_{Zn} + Zn_i$), Schottky pairs (3) V_O and V_{Zn} ($V_O + V_{Zn}$ Types I and II; described here) and (4) V_O Zn_i ($V_O + Zn_i$), and (5) V_{Zn} clusters are treated.

II. COMPUTATIONAL DETAILS

First-principles calculations were performed using the projected augmented plane-wave[25] method as implemented in the Vienna *ab initio* simulation package.[26] We have performed calculations for supercells of sizes varying from 32 to 256 atoms. The defects are simulated by adding and/or removing constituent atoms to and/or from the supercell. We have tested the total energy convergence with respect to **k** points and plane-wave energy cutoff. For the sake of more accurate results we used a plane-wave energy cutoff of 550 eV. Brillouin-zone sampling was done in the Monkhorst-Pack scheme with a **k**-point mesh of $3 \times 3 \times 3$ for smaller supercells and $2 \times 2 \times 2$ for supercells with 192 and 256 atoms. Optimization of the atomic geometry was performed via a conjugate-gradient minimization of the total energy, using Hellmann-Feynman forces on the atoms and the stresses in the unit cell. During the simulations, atomic coordinates and axial ratios were allowed to relax for different volumes of the unit cell. Convergence minimum with respect to atomic relaxations was assumed to have been attained when the energy difference between two successive iterations was less than 10^{-6} eV per unit cell and the forces acting on the atoms were less than 1 meV Å^{-1}. For charged defects a jellium background charge was used. Exchange and correlation effects are treated under the generalized gradient approximation (GGA)[27] including the Perdew-Burke-Ehrenkof (PBE) functional.

A. Defect formation energy

To find out the most abundant defect or defect complex, we have calculated the formation energy for all the aforementioned defect types. The ZnO crystal is assumed to be in equilibrium with a reservoir of Zn and O. The formation energy of a defect with charge q is given by

$$\Delta H^{\mathrm{def}}(q) = E_{\mathrm{tot}}^{\mathrm{def}} - E_{\mathrm{tot}}^{\mathrm{bulk}} \pm \sum_i n_i \mu_i + q[E_V + E_F], \quad (1)$$

where $E_{\mathrm{tot}}^{\mathrm{def}}$ is the total energy of the supercell containing a defect in the charge state q and $E_{\mathrm{tot}}^{\mathrm{bulk}}$ is the total energy of the ideal supercell. We define the difference between $E_{\mathrm{tot}}^{\mathrm{def}}$ and $E_{\mathrm{tot}}^{\mathrm{bulk}}$ as the configuration energy E_{conf}. E_F is the Fermi energy and E_V is the valence-band maximum (VBM) of the ideal crystal. n_i indicates the number of atoms of type i that have been added to ($n_i > 0$) or removed from ($n_i < 0$) the supercell when the defect is created. The μ_i are the corresponding chemical potentials of the defect species that determine the flow of atoms between the atomic reservoirs and the host crystal. The chemical potentials of the atoms involved depend on the experimental growth conditions, that is, Zn rich or O rich. Hence they are considered as variables implying that ZnO can be experimentally grown under varying Zn/O ratios. However, the chemical potentials are placed with some bounds in thermodynamic equilibrium. Under maximum Zn-rich conditions, μ_{Zn} is equivalent to the energy of the metallic Zn. This upper bound on μ_{Zn} results in a lower bound on μ_O. Hence, μ_{Zn} and μ_O are assumed under zinc-rich conditions to be $\mu_{Zn} = \mu_{Zn(bulk)}$ and $\mu_O = \mu_{ZnO} - \mu_{Zn}$. Similarly, under maximum O-rich conditions, the chemical potential of oxygen is bound by the energy of O in an isolated O_2 molecule and leads to a lower limit on μ_{Zn}. Thus under oxygen-rich conditions, limit $\mu_O = 1/2\mu_{O_2}$ and $\mu_{Zn} = \mu_{ZnO} - \mu_O$.

The last term in Eq. (1) determines the energy required to remove (add) q electrons from (to) the defect to (from) the electron reservoir, that is, the Fermi energy of bulk ZnO. To understand the electronic behavior of defects, it is useful to examine the formation energy of defects as a function of Fermi energy E_F. The E_F is referenced to the VBM and varies from 0 to the band gap (E_g).

The energy required to change the charge state of a thus-formed defect (defect transition energy) is defined as

$$\epsilon(q/q') = [\Delta H(q) - \Delta H(q')]/(q' - q), \quad (2)$$

where q and q' are two different charge states of the defect. Owing to this transition, there are often transition levels induced in the band gap of semiconductors that correspond to the thermal ionization energies.[31] The experimental significance of such levels is that they imply the relative stability of a particular charge state (q or q') corresponding to the Fermi level position $\epsilon(q/q')$.

As the formation energy is calculated by using periodically repeated finite-sized supercells, artificial long-range elastic and electrostatic interactions between the periodic defect images can be introduced. However, when supercells of sufficiently large sizes are used, the interaction of the defect with the spurious periodic images and with the jellium background will become negligible.[32] Hence we used 192-atom supercells in most cases and, also, supercells with 256 atoms in some selected cases. Finite-size effects are taken into account in the formation energy calculations by considering the change in configuration energy ($E_{\mathrm{conf}} = E_{\mathrm{tot}}^{\mathrm{def}} - E_{\mathrm{tot}}^{\mathrm{bulk}}$) and extrapolating to infinity.

Makov and Payne[33] proposed that the total energy of a defect-containing supercell should scale as $1/L$, where L is the linear length scale of the supercell. This is because the spurious monopole electrostatic term representing the interaction of the net charge of the point defect with the neutralizing background charge density is dominant. Paudel and Lambrecht[20] carefully analyzed the dependence of the total energy with respect to the radius of a sphere (R) whose volume is equal to that of the supercell. They found that relaxation and electrostatic effects appear to compensate each other to some extent and the results do not support a dominant $1/R$ behavior. As the range of treatable supercell sizes is too small, it is not clear whether a $1/R$ or $1/R^3$ behavior provides a better fit.

The calculated band gap (E_g) of 0.9 eV is considerably smaller than the experimental value of 3.24 eV at room temperature. In particular, as the defect formation energies depend on E_F, they can be severely affected by the underestimation of E_g. Therefore, several correction schemes have been reported by many authors such as an extrapolation scheme[9] and correction by the LDA + U method.[11,34] The influence of different band-gap correction schemes on the formation energy of defects was analyzed elaborately in Refs. 23 and 24. In contrast, Oba *et al.*[10] did not use any corrections since the relative values of the formation energies remain quantitatively identical for the entire Fermi energy range. We have adapted a correction method proposed by Lany and Zunger,[12] in which the VBM is shifted downward by an amount (equivalent to the downward shift of the VBM obtained from the GGA + Uq calculation), and the is shifted by the remaining band-gap error as given in the following.

The well-known LDA band-gap error is corrected by acknowledging that the Zn-d states are too shallow because of their strong self-interaction. It has been shown earlier[35] that the E_g value and the position of the Zn-3d band can be significantly improved by using an LDA + U calculation with a U value of 10 and $J = 0$ eV. The Zn-3d states exist at -5 eV from the VBM in the usual LDA calculations. Owing to the inclusion of correlation effects, they are pushed down to -7.5 eV from the VBM, whereas the experimental photoemission spectra[36,37] point to this state's being in the range of -8.5 to -8.8 eV. This d-band lowering weakens the repulsion of d states with oxygen-p orbitals and lowers the energy of the VBM. Thus the E_g value increases to 1.84 eV in the present GGA + U calculation, compared to 0.90 eV from the usual GGA calculation. We determine the correction ΔE_V for the energy of the VBM as the difference in the VBM of a pure host obtained from the GGA + U versus the GGA, measured with respect to the anion-s-like Γ_1 state. Thus E_V in Eq. (1) is corrected by $\Delta E_V = -1.06$ eV and the remaining discrepancy in the E_g value (ΔE_c) is taken care of by performing a scissor operation (i.e., shifting the CBM upward equivalent to the experimental band gap).

In line with Refs. 12 and 13, for defects that introduce electrons in perturbed host states, like shallow donors, a correction $n\Delta E_c$ is applied to the formation energy when the perturbed host state is occupied by n electrons, because the donor perturbed host state is assumed to shift along with the host CBM during band-gap correction. This procedure is adapted for Zn_i and Zn_O, which are found to be shallow donors among the different types of defects considered in the present study. In contrast, for defects that introduce localized levels in the band gap, no such corrections are included because the localized levels are not expected to follow the band edges during band-gap correction. We use the GGA + U scheme only to obtain the correction for the host band edges.

III. RESULTS AND DISCUSSION

First, we consider the structural properties of pure ZnO. Even though ZnO mostly crystallizes in hexagonal wurtzite-type structures, it can also be stabilized in the cubic zinc-blend structure by epitaxial growth of ZnO on suitable cubic substrates.[38] Therefore, we have performed complete structural optimization in both structural variants and found that the wurtzite-type hexagonal structure is slightly lower in energy. Hence we considered the wurtzite-type structure for studying various defects. However, for V_O alone we performed the calculations in zinc-blend structures also (discussed later). As these two structure types are energetically close, the results obtained from the present study can also be used to understand the zinc-blend-type structure.

The optimized lattice parameters for pure ZnO are $a = 3.2883$ (3.249) and $c = 5.3057$ (5.206) Å (values in parentheses are the corresponding experimental ones, from Refs. 28–30). These parameters are used to construct the supercells. The calculated formation energy for pure ZnO is -3.28 eV/f.u. This value is comparable to the experimental enthalpy of formation of -3.57 eV/f.u. The properties of native defects depend on the chemical potentials of constituent atoms. Hence we have calculated the formation energy of metallic Zn in a hexagonal structure by including an energy cutoff of 800 eV and 40 **k** points. The optimized lattice parameters are $a = 2.6699$ (2.6647) and $c = 4.9417$ (4.9469) Å. The calculated cohesive energy is -1.3447 (1.359 eV/Zn). For oxygen, an isolated oxygen molecule was considered inside a 20-Å cubic cell for computational purposes. The calculated bond length is 1.23 (1.21) Å and the cohesive energy is -4.48 eV/atom (-5.17 eV/atom).

Now let us discuss the supercell size effect. To study point defects like V_O, V_{Zn}, O_i, and Zn_i, we have constructed supercells with 72, 108, 128, 192, and 256 atoms and performed complete structural relaxations (stress as well as force minimizations). As the range of supercell sizes computationally treatable is small, Paudel and Lambrecht[20] noted that it is not clear whether the formation energy should be scaled with the inverse of length or volume of the supercells. However, the inverse volume scaling does not introduce extra fitting parameters, and extrapolated values do not differ much from those of the largest cells. As this scaling also allows us to extract the energies of formation in the dilute limit, this method has been adapted.

The calculated formation energy of V_O in different charge states as a function of the inverse volume is shown in Fig. 1. The extrapolated formation energy for neutral V_O is almost the same as that for the largest cell (with 256 atoms), and those for V_O^+ and V_O^{2+} differ by less than 0.05 eV. This indicates that both the Madelung-type correction and the valence band alignment correction for this defect are unimportant.[39] For primary defects we adapted the aforementioned procedure. For more complex defects such as $V_O + O_i$ (simultaneous

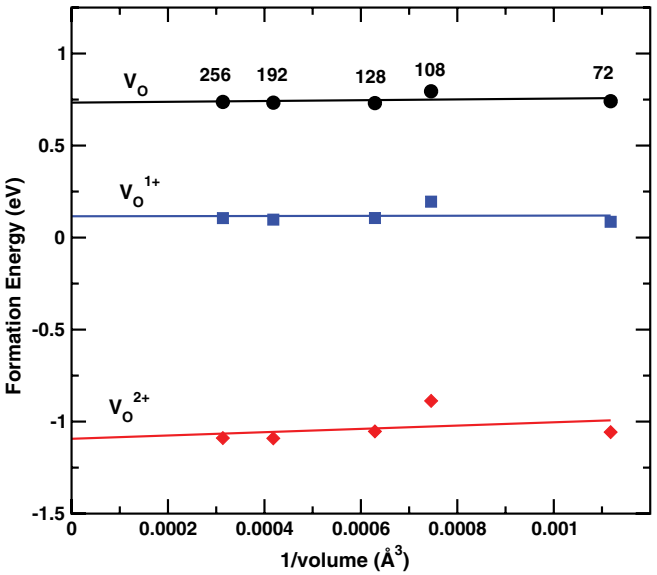

FIG. 1. (Color online) Calculated formation energy of V_O for various supercell sizes. The formation energy is calculated for Zn-rich conditions and E_F is at the VBM.

presence of V_O and O_i), we used large supercells, consisting of 192 atoms, owing to constraints in computational resources. When V_O and O_i are close to each other (at 2.1 Å), O_i migrates into the V_O site during relaxation. To avoid this, they were placed about 6.5 Å apart. As the formation energy of V_O for the 192-atom supercell does not differ much from the extrapolated value, the uncertainty involved in this procedure is considered to be negligible.

The formation energies of the isolated point defects under the limiting chemical potentials of Zn-rich and O-rich conditions at the VBM are listed in Table. I. Under Zn-rich and p-type (E_F close to the VBM) conditions, V_O^{2+} is the most dominant defect. We checked the relative stability of V_O with different charge states in zinc-blend structures also. The calculated values are 0.67, 0.25, and −1.10 eV for V_O^0, V_O^{1+}, and V_O^{2+}, respectively, under Zn-rich conditions. Similarly for O-rich conditions, these values are 4.05, 3.63, and 2.28, respectively. It can be seen that the formation energies of V_O in wurtzite and in zinc-blend-type structures are similar, implying the same relative stability of the defects in the two structures.

Above V_O, Zn_O^{4+}, and Zn_i^{2+} have the next lower energies; all the other defects have at least 2.2 eV higher formation energies. It can be noted that V_O remains dominant under n-type conditions (E_F closer to the CBM) also, where Zn_O^{2+} and Zn_i^{2+} have lower energies than the ($V_O + Zn_i$) complex.

In contrast, under O-rich conditions V_{Zn} (in all charged states) has the lowest formation energy. V_O^{2+} is 0.36 eV higher in energy than V_{Zn} under p-type conditions. Even though Zn_i is one of the dominant defects under Zn-rich conditions, this is not the case for O_i under O-rich conditions. In fact, V_O is more dominant than O_i under O-rich conditions also. However, the O_{Zn} in the 2 charge state is lowest in energy among all defects under n-type conditions, implying that it could act as the compensating center.

Table II shows that ($V_O + Zn_i$) in the 4+ charge state is the second most dominant defect after V_O^{2+}. As Schottky pairs involve the simultaneous presence of V_O and V_{Zn}, their formation is independent of the chemical potential of Zn and O. This is also the case for Frenkel pairs, with the simultaneous presence of a vacancy and an interstitial defect. It is interesting to note that the binding energy of Frenkel pairs is higher than that of Schottky pairs. Among the stable defect complexes, ($V_O + V_{Zn}$) Type I has the lowest formation energy. Moreover, the ($V_O + V_{Zn}$) defect (acting as the recombination center) has a lower formation energy than O_i (acceptor-type defect), suppressing p-type doping of ZnO. However, it should be noted that these values are obtained without applying any correction. The situation changes significantly upon applying band-gap correction, as discussed here.

TABLE I. Formation energies of elementary defects in ZnO without band-gap corrections. Values are given for Zn-rich and O-rich conditions at $E_F = 0$ eV (valence-band maximum; VBM) and $E_F = 0.90$ eV (conduction-band minimum; CBM).

		Zn-rich conditions		O-rich conditions	
Defect	Charge state	VBM	CBM	VBM	CBM
V_O	0	0.73	0.73	4.11	4.11
	1+	−0.11	0.68	3.27	4.05
	2+	−1.19	0.33	2.19	3.75
V_{Zn}	0	5.21	5.21	1.83	1.83
	1−	7.05	6.27	1.90	1.11
	2−	8.84	7.28	1.93	0.34
O_i	0	7.25	7.25	3.86	3.86
	1−	9.03	9.83	5.65	6.41
	2−	11.32	12.86	7.94	9.51
Zn_i	0	2.07	2.07	5.45	5.45
	1+	1.27	2.22	4.65	5.43
	2+	0.61	2.02	3.99	5.49
Zn_O	0	2.14	2.14	8.91	8.91
	1+	1.37	2.12	8.13	8.93
	2+	0.53	2.08	7.29	8.88
	3+	0.50	10.40	7.26	17.27
	4+	0.44	13.78	7.20	20.09
O_{Zn}	0	11.66	11.66	4.89	4.89
	1−	12.33	8.99	5.56	2.19
	2−	13.06	6.34	6.30	−0.34
$O_{Zn} + Zn_O$ pair	0	7.26	7.26	7.26	7.26
	1+	8.65	12.17	8.65	12.17
	2+	10.86	17.62	10.86	17.62

A. Zn-rich conditions

Since the formation energies of charged defects depend on the Fermi level position, they are given as a function of E_F under Zn-rich [Fig. 2(a)] and O-rich [Fig. 2(b)] conditions. Kinks in the curves correspond to transitions between different charge states of a particular defect, which can be applied to estimate positions of defect levels within the band gap.

As the E_g value almost doubles in the GGA + U calculation, the energetics of defect formation also vary considerably, especially the relative stability of the higher defect charge states. While the uncorrected formation energies indicate that V_O is the dominant defect among all those considered,

TABLE II. Formation energies of native defect complexes in ZnO without band-gap corrections. Values are given for Zn-rich and O-rich conditions at $E_F = 0$ (valence-band maximum; VBM) and $E_F =$ 0.90 eV (conduction-band minimum; CBM).

		Zn-rich conditions		O-rich conditions	
Defect	Charge state	VBM	CBM	VBM	CBM
$(V_O + Zn_i)$	0	6.57	6.57	13.33	13.33
	1+	3.97	3.61	10.77	11.50
	2+	2.69	3.54	9.46	10.90
	3+	1.03	3.36	7.79	10.05
	4+	0.21	3.17	6.97	10.00
(V_O+V_{Zn})					
Type I	0	3.15	3.15	3.15	3.15
	1+	3.04	3.81	3.04	3.81
	2+	3.11	4.67	3.11	4.67
Type II	0	4.39	4.39	4.39	4.39
	1+	4.19	4.98	4.19	4.98
	2+	4.27	5.77	4.27	5.77
$(V_O + O_i)$	0	5.59	5.59	5.59	5.59
	1+	5.04	5.80	5.04	5.80
	2+	4.89	6.45	4.89	6.45
$(V_{Zn} + Zn_i)$	0	4.54	4.54	4.54	4.54
	1+	4.33	5.12	4.33	5.12
	2+	4.42	5.98	4.42	5.98
$2(V_{Zn})$	0	11.09	11.09	4.33	4.33
$3(V_{Zn})$	0	16.82	16.82	6.68	6.68

the corrected values [Fig. 2(a)] indicate that Zn_O^{4+} is the lowest-energy defect, at least for E_F values from 0 (VBM) to 0.23 eV. For E_F above 0.23 eV and up to the CBM, V_O is the dominant defect. It can be seen that the 2+ to 0 transition of V_O takes place at 1.4 eV below the CBM, indicating that it is a deep double donor. This finding is in good agreement (1.2 eV below the CBM) with a density function theory study[21] using a hybrid functional that correctly reproduces the experimental band gap of ZnO. A more recent hybrid functional calculation[22] using PBE0 has also found V_O at 1.2 eV below the CBM. In addition, the calculated formation energy for V_O^0 (0.73 eV) is in good agreement with a report[19] based on *a posteriori* band-gap correction as well as with Ref. 21, with PBE0 calculations that obtained 0.8 and 0.9 eV, respectively. Our calculated formation energy of V_O^{2+} at the VBM (−3.35 eV) is in close agreement with that (−4.0 eV) obtained from the PBE0 functional.[22] This low formation energy of V_O promotes nonstoichiometric ZnO.

Moreover, the 1+ to 0 transition of V_O^+ occurs at 1.5 eV from the CBM. As shown in many previous studies,[9,12,63] V_O exhibits a negative-U character, with the 1+ charge state being unstable in the entire E_F range, with a U value of 0.11 eV. The metastable behavior of V_O^{1+} is experimentally confirmed by optical detection of electron paramagnetic resonance spectroscopy.[64] As our calculated values for formation energy and transition levels are in good agreement with a previous study[21] that reproduced the experimental value of E_g, the same procedure is used to understand the effect of other defects.

The 4+ to 3+ transition of Zn_O occurs at 1.9 eV below the CBM (explained in the next section) and the subsequent 3+ → 2+, 2+ → 1+, and 1+ → 0 transitions occur at 0.77, 0.06, and 0.05 eV from the CBM. Especially, the 2+ to 1+/0 transition occurring close to 0.05 eV below the CBM classifies this defect as a shallow donor and one of the dominant contributors to n-type conductivity in ZnO. The 2+ to 1+ transition of Zn_i occurs at 0.16 eV below the CBM, and the 1+ to 0 transition of Zn_i occurs 0.05 eV below the CBM. Since both Zn_O and Zn_i have charge state transitions close to the CBM, it is obvious that these two defects are shallow donors, in agreement with previous studies, and main contributors to n-type conductivity under extremely pure conditions. However, these defects have a higher formation energy than the V_O^0 state. Hence these defects may donate electrons in

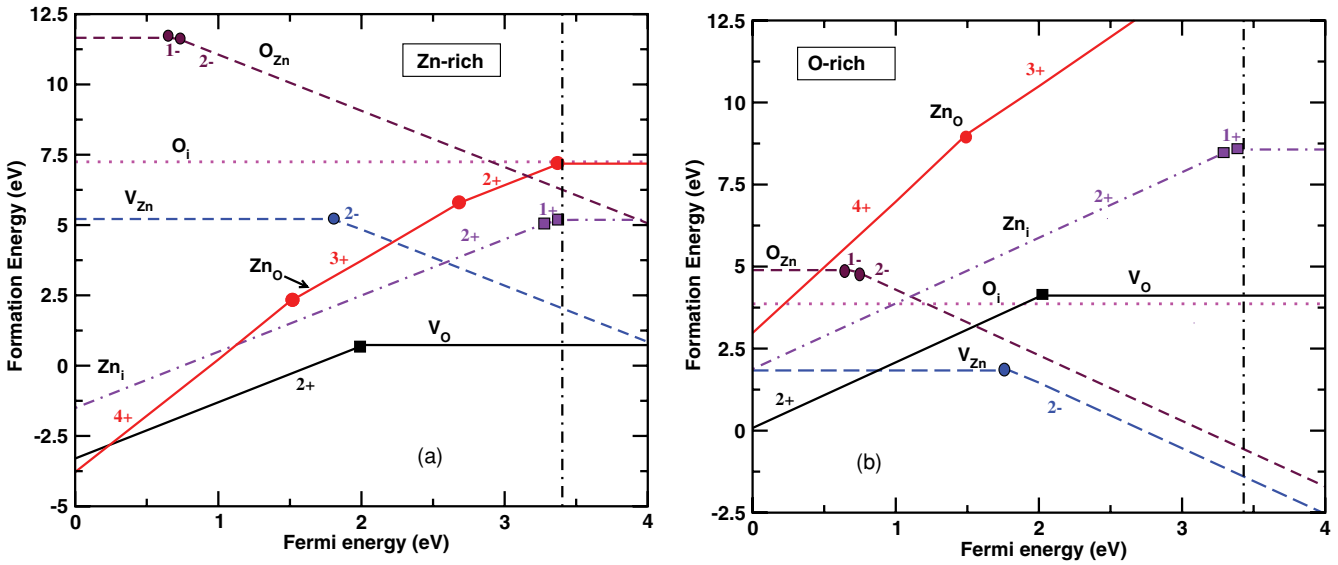

FIG. 2. (Color online) Formation energy of simple intrinsic defects in different charge states as a function of Fermi energy: (a) under Zn-rich conditions and (b) under O-rich conditions. Appropriate band-gap corrections are included (see text). The dashed vertical line indicates the conduction-band minimum, and circles and squares indicate charge-transition points.

higher-energy processes and nonequilibrium conditions. In fact, a shallow level at 0.03 to 0.06 eV below CBM has been observed in Zn-rich samples by different experimental techniques[40–42] and suggested to originate from H and/or Al impurities or Zn interstitials. As the role of H and Al is not considered in the present study, they cannot be excluded, but the present study indeed suggests that Zn_i and Zn_O are strong candidates to act as shallow donors in pure ZnO samples.

It is well known that both Zn and O can occupy octahedral and tetrahedral interstitial sites in ZnO. However, we considered only octahedral interstitial sites, as the formation energy of tetrahedral sites has been shown in earlier work[10] to be always higher than the former. Even though V_{Zn}^0 has a higher energy of formation (ca. 6.68 eV) than Zn_i under p-type conditions, the 2− charge state becomes very much lower in energy than the shallow donors Zn_i and Zn_O closer to the CBM. This indicates that V_{Zn} does not contribute to p-type conductivity in ZnO but, rather, acts as a deep compensating center. The O_i in neutral states is stable throughout the E_F range, with a formation energy of 7.23 eV.

As V_O and Zn_i are often cited as the dominant intrinsic defects, we checked the stability of defect complexes formed between them. In our structural model V_O and Zn_i are placed at least 6.4 Å apart. When they are placed close to each other, Zn atoms as far as second-nearest neighbors were significantly displaced from their equilibrium positions after structural relaxation. The Zn-antisite (Zn_O) defect can, in a way, be viewed as the ($V_O + Zn_i$) complex, because we found off-site displacement of Zn atoms from the V_O, in line with Refs. 14 and 18. The surrounding Zn atoms of Zn_O move away from their equilibrium positions, and one of the Zn atoms occupies an antibonding interstitial ($AB_{Zn,||}$) site. In the structural model we considered for ($V_O + Zn_i$), although one of the nearest-neighbor Zn atoms moves very close to the V_O, the Zn_i remains at the octahedral interstitial site. Hence we call the ($V_O + Zn_i$) complex ($V_O + Zn_i$)-far. This complex is 3.0 eV higher in energy than V_O. Among the five types of defect complexes considered, $(V_O + Zn_i)^{4+}$ has the lowest energy (0.4 eV) under p-type conditions (E_F close to the VBM). Interestingly the 1+ to 0 transition of this defect complex takes place at 0.6 eV below the CBM despite being a high-energy transition at 6.6 eV. A level at 0.32 eV below the CBM has been observed in earlier[44] as well as recent[42,43] reports and has been attributed to an oxygen-vacancy complex. Moreover, dielectric loss peaks have been observed[61] in single-crystal ZnO with an activation energy of 0.36 eV, and V_O is believed to cause the peak. The binding energy of the ($V_O + Zn_i$)-far complex calculated from the formation energy with E_F at the VBM, shows a negative value. However, the attractive interaction between V_O and Zn_i in the ($V_O + Zn_i$) complex is suggested[62] to lead to n-type conductivity in ZnO. It may be noted that in Ref. 62, the charge state of this complex is assumed to be 2+ and the Fermi level is fixed at the deep donor level of V_O. Hence the stability of this complex studied as a function of the separation between the defects for different charge states, including complete structural relaxation, may shed more light on the stability and defect levels of this complex.

The simultaneous presence of V_O and V_{Zn} ($V_O + V_{Zn}$) is considered in two variants, that is, nearest-neighbor vacant sites (Type I) and vacant sites 4.57 Å apart (Type II). Of these two variants, the Type I complex has the lower formation energy. All the defect complexes, except ($V_O + Zn_i$), have a positive binding energy (0.8 to 0.95 eV at the VBM). The charge transitions of these defect complexes are deep, within 1–2 eV above the VBM. The antisite pair ($O_{Zn} + Zn_O$) is slightly higher in energy (7.26 eV) than O_i in the neutral state and has 0 to 1− and 1− to 2− transitions occurring at 1.81 and 1.38 eV below the CBM, respectively. In fact, among the defect complexes considered, only the antisite-pair complex has an acceptor-type character at the CBM and could contribute to compensating the n-type carriers. Oxygen at a Zn site (O_{Zn}) has the highest energy of formation among all the defects considered and is also seen to be a deep acceptor under Zn-rich conditions.

B. O-rich conditions

Similar to that under Zn-rich conditions, the role of band-gap correction is also significant for defect formation energies under oxygen-rich conditions. The uncorrected formation energy values indicate that V_{Zn} and O_{Zn} have the lowest energies at VBM and CBM, respectively. However, upon including the E_g correction, V_O^{2+} becomes the lowest-energy defect under p-type conditions. As the donor-type defect (hole killer) V_O^{2+} is dominant under p-type conditions under both Zn-rich and O-rich conditions, it may explain why it is difficult to accomplish p-type ZnO. It is interesting to note that for E_F below ($E_{VBM} + 1.0$) eV, both Type I and Type II ($V_O + V_{Zn}$) defects have a lower energy than O_i even under O-rich conditions [see Figs. 2(b) and 3].

Even though V_{Zn} has a high formation energy (1.83 eV) close to the VBM, its formation energy decreases when the Fermi level increases, as expected for acceptor-type defects. However, the (0/2−) charge transition occurs deep inside the band gap (at 1.81 eV above E_{VBM}) as found by photoluminescence study.[69] Hence V_{Zn} acts as a compensating center under

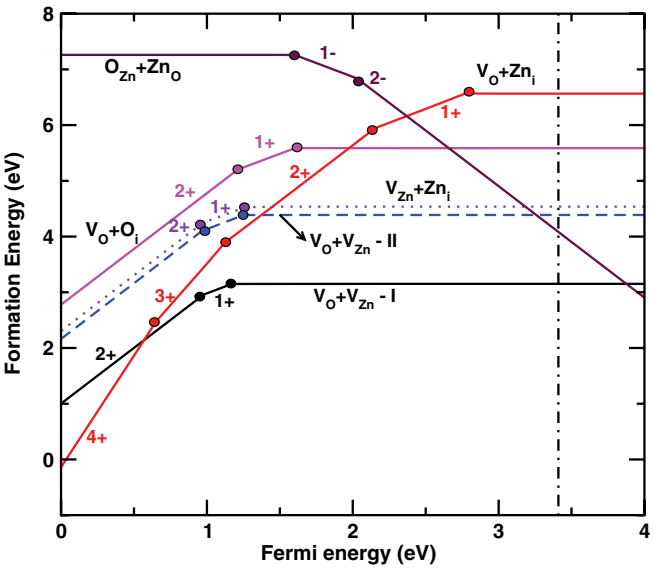

FIG. 3. (Color online) Formation energy of intrinsic defect complexes in different charge states as a function of Fermi energy (under Zn-rich conditions). The formation energy of defect complexes [except for ($V_O + Zn_i$)] is independent of synthetic conditions and the band gap is corrected (see text).

n-type conditions rather than as a shallow acceptor. Figure 2(b) shows that the V_{Zn} is the dominant defect for most of the Fermi energies considered. This finding is in agreement with earlier theoretical studies.[16,18,21] Using positron annihilation spectroscopy, Tuomisto *et al.*[65] identified V_{Zn} as a dominant defect in n-type ZnO. Furthermore, in combination with isochronal annealing of electron-irradiated samples, they found a second acceptor, suggesting it to be either O_i or O_{Zn}. Though the O_{Zn} defect exhibits a high formation energy under p-type conditions, it is the next-lowest-energy defect (after V_{Zn}) under n-type conditions and behaves like a compensating center similar to V_{Zn}. Hence, even though O_i has a lower formation energy than O_{Zn} under p-type conditions, the reverse is true for $E_F \geqslant 1.3$ eV. Thus O_{Zn} may be the second acceptor-type defect in n-type ZnO as suggested by Tuomisto and co-workers.

The defects Zn_O, Zn_i, and $(V_O + Zn_i)$ have low formation energies under Zn-rich conditions (Fig. 2). But these defects have high formation energies under O-rich conditions. Even though charge transitions of these defects occur close to the CBM, n-type conductivity cannot be readily attributed to them under ambient conditions due to their high formation energies. However, the defect complexes $(V_O + V_{Zn})$, $(V_O + O_i)$, and $(V_{Zn} + Zn_i)$ have the same energy of formation under both Zn-rich and O-rich conditions. Moreover, all these defect complexes have charge transitions occurring inside the band gap and do not give rise to shallow states.

C. Origin of luminescence

The calculated charge transition energy according to Eq. (2) corresponds to a position of the zero-phonon line in the case of defect-related photoluminescence or photoluminescence excitation and is close to the thermal ionization energy in experiments such as photoluminescence and deep-level transient spectroscopy.[45] Based on this concept, attempts have been made to explain GL in ZnO[9] and YL in GaN.[46] The optical transitions have also been extracted[12,47] from the formation energy of defects in specific charge states by fixing the atomic configuration of the initial charge state according to the Frank-Condon principle.

The exciton structure in ZnO should involve a relatively localized hole state and a rather delocalized electron.[48] Upon interaction with a defect, a process of recombination of the localized electron of the defect with a hole component of the exciton could occur. For such a process, the luminescence is expected to be characterized by energies close to the calculated defect levels. On the contrary, upon ionization of the defect (loss of an electron to the conduction band), the electron component of the exciton could recombine with a hole, which is now localized on the defect. In this case, there will be some reduction in the emission energy compared to the ionization energy (Stokes shift). The optical transition energy is the summation of ionization energy and atomic relaxation energy. The optical transition is shown to be close to the thermodynamic transition energy when the atomic relaxation energy is low.[49]

As the considered defect complexes are possible candidates for the luminescence peaks in the visible range of undoped ZnO samples, they are considered in detail (Fig. 3). We performed structural relaxation of a defect complex in a specific charge state, say, q with the initial atomic configuration of charge state $q + 1$. The atomic relaxation energy for the defect

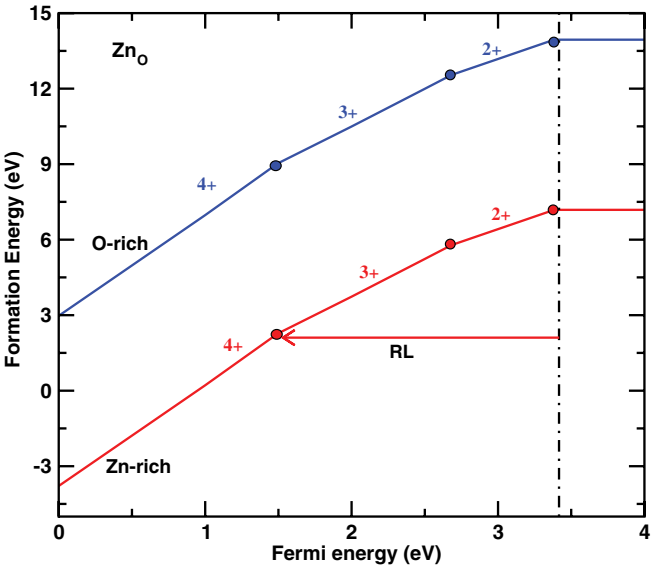

FIG. 4. (Color online) Charge transition levels of Zn_O under Zn-rich and O-rich conditions. The energy level responsible for red luminescence is shown by the arrow.

complexes considered in this study is calculated to be in the range of 0.07–0.12 eV. As the relaxation energies are relatively low, the calculated thermodynamic transition levels can be qualitatively used to understand the different luminescence peaks observed in ZnO.

The 4+ to 3+ transition of Zn_O occurs at 1.9 eV below the CBM. Hence the red/orange photoluminescence band at 1.902 eV may be attributed to this transition. Interestingly, the red/orange coloration has been shown[50,51] for as-prepared samples and those annealed under Zn vapor. The samples become transparent upon annealing under O vapor and the red coloration is reversible. As the formation energy of Zn_O in the 4+ state is negative (Fig. 4), it can readily form under Zn-rich conditions, and the 4+ to 3+ transition can take place under ambient conditions. In contrast, the formation energy of Zn_O under O-rich conditions is higher than that of other defects considered. Hence the attribution of red color to the 4+ to 3+ transition of Zn_O under Zn-rich conditions is reasonable.

The orange luminescence of ZnO can be attributed to the 1+ to 0 transition (2.1 eV below the CBM) of the $(V_{Zn} + Zn_i)$ and $(V_O + V_{Zn})$-II complexes, even though these complexes require more formation energy compared to the $(V_O + V_{Zn})$-I complex.

YL is also observed in ZnO and it has been observed in undoped samples as well as samples doped with Al, H, Li, and N.[8] The YL is commonly attributed to a defect state involving Zn vacancies. In photoluminescence spectra of Ga-doped ZnO layers, a dramatic decrease in the YL band intensity was observed,[52] where Ga substitutes for Zn in ZnO, so that the concentration of V_{Zn} is reduced. Stable complexes of V_{Zn} can be expected in ZnO similar to the V_{Ga}-related complexes in GaN.[53] In particular, V_{Zn} is likely to form stable complexes with shallow donors in ZnO[54] and such a complex is cited as a possible reason for YL. However, the defect complex of V_{Zn} together with the shallow donor Zn_i $(V_{Zn} + Zn_i)$ is a possible candidate for the orange luminescence as already mentioned.

The intensity of YL observed in a ZnO sample prepared by rf magnetron sputtering increases as n-type conductivity decreases[60] and deep acceptor-like defects are noted as the reason for YL. Our results suggest that the 1+ to 0 transition of the $(V_O + V_{Zn})$-I defect complex occurs at 2.2 eV below the CBM, which can cause the YL. It can be recalled that V_{Zn} rather acts as a compensating center. So when a complex between V_O and V_{Zn} is formed, it can lead to YL and reduce the n-type conductivity.

The often observed GL in ZnO is a subject of major controversy. The origin of GL has been attributed to various sources, such as V_O, V_{Zn}, donor-acceptor complex[70], and copper impurities(see, e.g., Ref. 59 and references therein). A hydrothermally grown ZnO single-crystal sample was shown to exhibit deep band emission at ca. 2.55 eV when annealed under Zn-rich conditions and high temperature, suggesting V_O to be the origin of GL.[55] An undoped ZnO sample also exhibited[56] GL under O-poor (Zn-rich) conditions and V_O is cited as the possible origin. As our calculations show charge transition of the $(V_O + V_{Zn})$-I complex from the 2+ to the 1+ state occurring at ca. 2.51 eV from the CBM, it could be the more appropriate origin of GL rather than V_O alone.

Moreover, Heo *et al.*[59] suggested that a transition from donor to deep acceptor (V_{Zn}) caused GL in ZnO films grown by molecular beam epitaxy. A time-resolved photoluminescence study[58] using pulsed laser excitation on a ZnO sample (not intentionally doped with any impurities) found the GL peak and suggested an intrinsic donor-acceptor pair complex as the possible reason for this peak based on the correlation between electron paramagnetic resonance and photoluminescence measurements. Especially, Ref. 58 suggests that the $(V_O + V_{Zn})$ complex in a specific charge state undergoes direct transition and emits light. Moreover, it is noted that the concentration of this complex would be lower than that of separate oxygen vacancies. As our energetics study indicates, the formation energy of the $(V_O + V_{Zn})$ complex is higher than that of V_O, the former would have a lower concentration under ambient conditions. It can be noted that GL is observed only upon excitation with a laser source with photon energies above E_g, in agreement with our study. Moreover, the samples that exhibited GL were found to be highly porous.[56] The optimized volume of the neutral $(V_O + V_{Zn})$ complex is 0.72% greater than that of the pure system, indicating more porosity. In addition, the GL is observed in oxygen-deficient, polycrystalline ZnO films grown by metal-organic chemical vapor deposition. As V_O is a deep-level donor, the transition between V_O and V_{Zn} donor-acceptor pairs is suggested[57] to cause GL. Based on the preceding arguments, we conclude that the $(V_O + V_{Zn})$-I complex could be the principal origin of GL in undoped ZnO.

In Ref. 58 a shift from a GL to a blue luminescence peak is observed when the intensity of the incident laser pulse is increased. In Fig. 2 the charge transitions (0 to 1− and 1− to 2−) at O_{Zn} can be seen to take place at ca. 2.5 eV from the CBM. Even though the formation energy of this defect is very high, the origin of blue luminescence may be assigned to these transitions because blue luminescence is observed only under a high-intensity laser pulse.

Since the defect formation energy is different under different growth conditions, various visible luminescence is observed in ZnO. In oxygen-rich samples orange luminescence has been observed,[56] while GL appears mainly in Zn-rich samples. The YL is observed[55] at ca. 2.37 eV in samples annealed under O-rich conditions. Even though elementary defects like V_{Zn} and V_O have a lower formation energy than defect complexes under O-rich conditions, the charge transitions of these defects may not give rise to luminescence. Similar to Zn-rich conditions, the 1+ to 0 transition of the $(V_O + V_{Zn})$-I complex could cause YL under O-rich conditions also. The 2+ to 1+ transition of the $(V_O + V_{Zn})$-I complex may be a likely candidate for the GL under O-rich conditions, as in the case of Zn-rich conditions.

D. Effect of oxygen vacancy on the lattice

As V_O is found to be dominant under both Zn-rich and O-rich conditions, the effect of this defect on crystal and electronic structures is discussed in some detail here. To understand the effect of V_O on the ZnO lattice, in Fig. 5 we show the charge density of pure ZnO and that with V_O in different charge states. Even though ionic bonding usually prevails for wide-band-gap semiconductors like ZnO, significant charge density contours can be seen between the Zn and the O atoms. In addition, the directional character of these contours implies a considerable covalent character of the bonding between Zn and O atoms. When one oxygen atom is removed, the surrounding Zn atoms have dangling bonds, the nearest-neighbor Zn atoms are relaxed toward the neutral vacancy site, and their bond lengths change by about 1%–3%. The volume of the cell decreases by 0.4% due to this inward relaxation of the Zn atoms. Figure 5(b) shows a uniform charge distribution around the V_O^0 contributed by the the surrounding

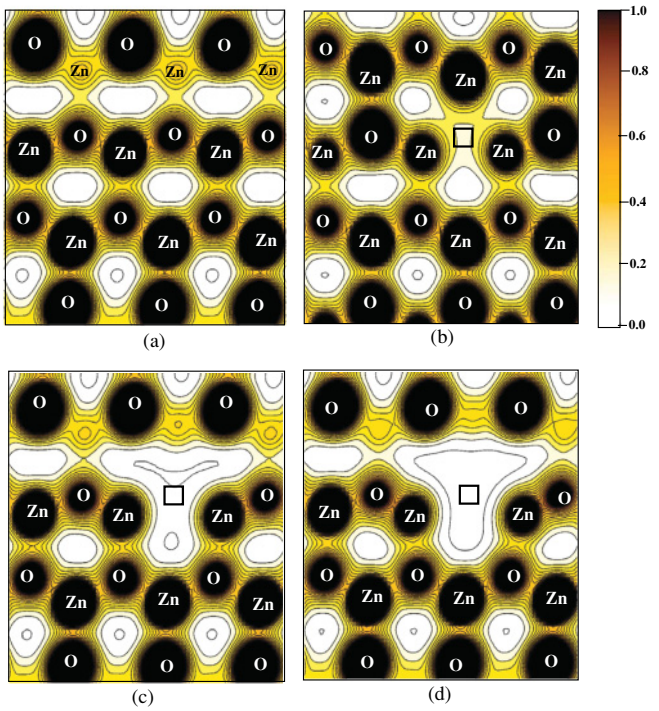

FIG. 5. (Color online) Charge density of ZnO: (a) pure, (b) with V_O, (c) with V_O^{1+}, and (d) with V_O^{2+}. The square indicates the oxygen vacancy site.

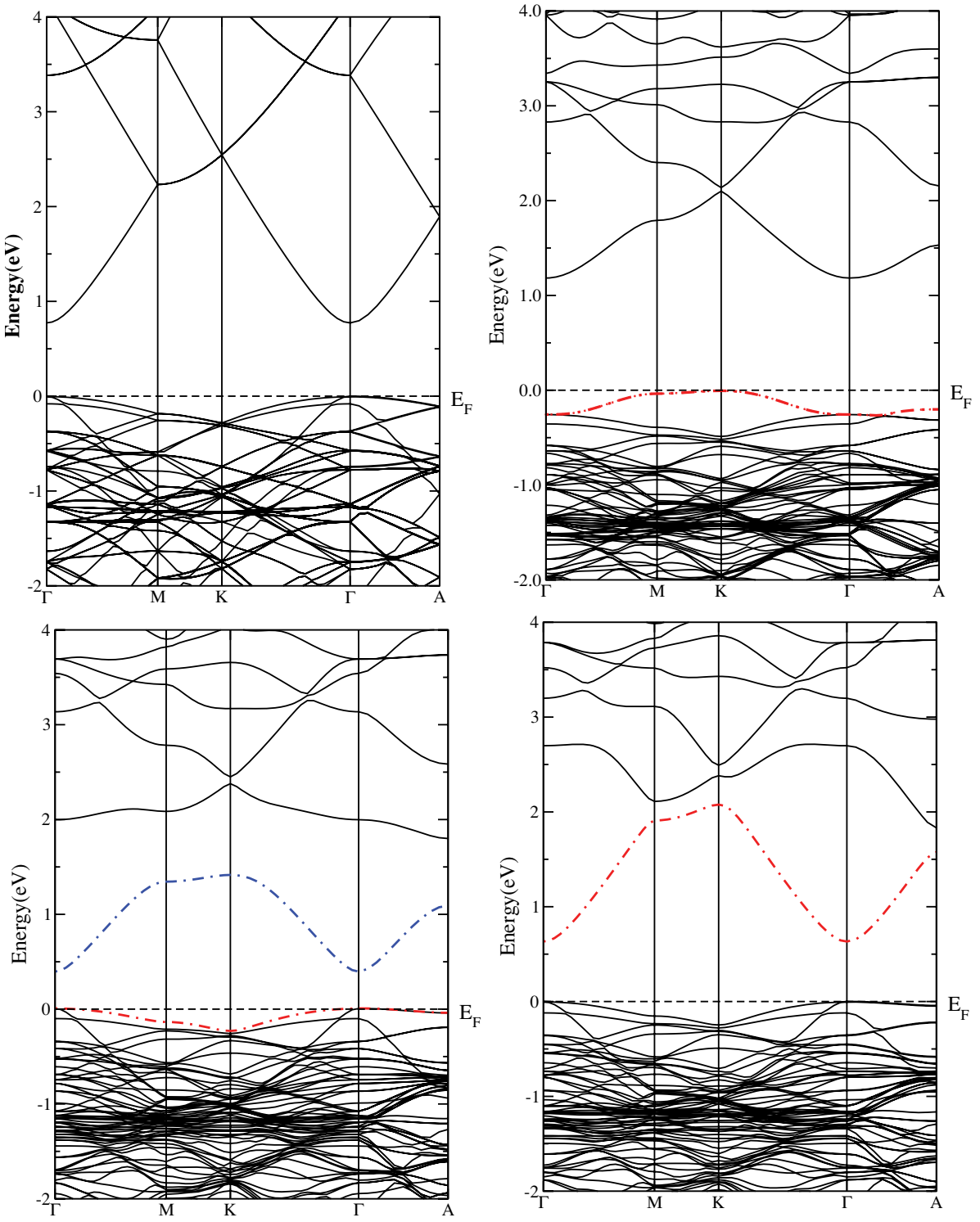

FIG. 6. (Color online) Electronic band structure of ZnO: (a) pure, (b) with V_O, (c) with V_O^+, and (d) with V_O^{2+}. The dashed line indicates the valence-band maximum and the dot-dashed bands arise due to defect.

Zn atoms. The electron-localization function[66] (which is a measure of the paired electron distribution) shows a maximum value at the vacancy site, also indicating presence of electrons at the vacancy site.

When the oxygen vacancy becomes singly charged (V_O^{1+}), the surrounding Zn atoms are repelled out and they relax outward. Therefore, the bond lengths of neighboring atoms undergo some 2%–7% change. Figure 5(c) shows some localized charge at the vacancy site. Moreover, an increase in the covalent interaction between the surrounding Zn atoms and their neighboring oxygen atoms is revealed from the dense charge density contours between them due to the reduction in their bond distances. There is a slight increase (0.1%) in the volume of the cell.

Owing to the doubly charged oxygen vacancy (V_O^{2+}), the first nearest-neighbor Zn atoms are further relaxed outward [Fig. 5(d)] and the bond lengths are changed by 2%–9%. The Zn–O bond length along the *ab* plane is reduced (1.91 Å) compared to that in the pure system (1.97 Å). Thus the covalent interaction between these atoms is increased and the cell volume decreases by 0.4 %, similar to the case with neutral V_O. This decrease in volume is similar to the decrease in the calculated[17] formation volume of neutral and 2+ charged V_O compared to that of 1+ charged V_O. The stronger covalent bond and reduced volume could be one of the reasons for the abundance of V_O under both Zn-rich and O-rich conditions.

To understand the effect of defects on the electronic structure of ZnO, we calculated the electronic band structure of ZnO using the full-potential linearized augmented plane-wave method as implemented in the Wien2K code.[67] We used a 72-atom supercell with 62 **k** points in the irreducible Brillouin zone. Other computational parameters used are similar to those in our previous work.[68] The band structure of pure ZnO shows an underestimated band gap of 0.78 eV and a direct gap at the Γ point. The number of bands is more due to the large number of atoms in the cell, thus making characterization of the bands difficult. Therefore density-of-states plots were also used for these analyses. In pure ZnO the VBM consists mainly of Zn-3*d* and O-2*p* bands [Fig. 6(a)]. As these orbitals are energetically degenerate, they hybridize, leading to dispersion of bands. The Zn *s* and *p* and O *s* electrons are also present in the energy range from −6 to −1 eV, but in negligible quantities. A broad band seen at the CBM arises due to *sp* hybridizatio.

In the case of the system with one neutral V_O, a very well-localized band at the top of the valence band is formed, resulting from the electrons contributed by the surrounding Zn atoms that are localized at the V_O^0 site. Owing to changes in the bond lengths, more hybridization of orbitals takes place, which can be inferred from the denser bands in the range of −1 to −2 eV. For the V_O^{1+} case, a partly filled band at the top of the valence band and an unoccupied defect level in the band gap are produced. As expected, a completely unoccupied defect level is created by the introduction of V_O^{2+}. The defect levels introduced in the band gap are highly dispersed (ca. 0.8 and 1.4 eV along Γ-*K* for V_O^{1+} and V_O^{2+}, respectively), which may be caused by the interaction among the vacancies repeated under three-dimensional periodic boundary conditions. A band-structure calculation[10] has found a similar dispersion of localized states for neutral vacancy, which is found to be decreased upon increasing the supercell size. A recent band-structure calculation[21] for the 192-atom cell using the HSE0 functional obtained a band dispersion of ca. 0.7 eV along the same Γ-*K* direction for the system with V_O^{2+}. This implies that the dispersion of the defect level arises due to the computational treatment. The character of unoccupied bands for the system with V_O^{2+} is similar to that for the pure ZnO system.

As Zn_i is found to be a shallow donor, we investigated the band structure for this defect in the charge states considered (not shown). The defect level introduced by Zn_i is partially occupied for neutral and +1 charge states and unoccupied in the 2+ state. The defect level has band dispersion features similar to the bottom-most conduction band of pure ZnO. Moreover, the character of this level is similar to that found for the V_O^{2+} case. Since V_{Zn} becomes a dominant defect under O-rich conditions, we studied the band structure related to this defect also. Some acceptor defect levels are created above the VBM. However, these levels are not as dispersive as the donor levels found for the cases of V_O^{2+} and Zn_i. The somewhat localized character of these acceptor levels increases the carrier effective mass, making it difficult to obtain *p*-type ZnO with a high hole mobility when V_{Zn} is present.

IV. CONCLUSIONS

First-principles calculations have been performed based on density functional theory to understand the effect of intrinsic defects in ZnO. We have considered point defects as well as intrinsic defect complexes. Complete structural optimizations of sufficiently large supercells with the considered defects were undertaken. The formation energy was calculated by extrapolation of the configuration energy with respect to the inverse of volume. Oxygen vacancy is found to be the dominant defect under Zn-rich conditions and also under O-rich conditions when $E_F \geqslant E_V + 1.0$ eV, and it is found to be a deep donor. The charge transition from 2+ to 0 takes place at 1.4 eV below the E_C and it exhibits a negative-*U* behavior, in agreement with recent hybrid functional calculations.

Among the considered intrinsic defects, Zn-interstitial and Zn-antisite defects are found to be shallow donors, however, with formation energies higher than that of V_O. Even though V_{Zn} has a lower formation energy at most Fermi energy values under O-rich conditions, the acceptor levels introduced by V_{Zn} and O_{Zn} are deep in the band gap. Both V_{Zn} and O_{Zn} instead act as compensating centers. Moreover, the holes give rise to narrow states in the VBM, leading to a high carrier effective mass. Hence it is difficult to achieve *p*-type conductivity only by intrinsic defects and their complexes.

The defect levels arising from the intrinsic defect complexes considered are present deep in the band gap and they can be responsible for the observed luminescence peaks in ZnO prepared under various conditions. The origins of some of the luminescence peaks are explored and the often observed GL may result from the $(V_O + V_{Zn})$ defect complex. The red/orange luminescence found in Zn-rich samples can arise from the Zn_O defect. YL may be caused by the $(V_O + V_{Zn})$ defect complex in Zn-rich and O-rich samples.

By performing charge density analysis and plotting the electronic band structure, we found that the formation of stronger covalent bonds between Zn and O atoms surrounding the doubly charged oxygen vacancy could promote the presence of V_O under Zn-rich and O-rich synthesis conditions when the Fermi energy is closer to the valence-band maximum. This could account for the nonstoichiometry frequently observed in ZnO. The *n*-type conductivity in ZnO can arise from Zn_i and Zn_O under nonequilibrium conditions like irradiation, and the coloration and photoluminescence peaks can arise from the intrinsic defect complexes.

ACKNOWLEDGMENT

The authors are grateful to the Research Council of Norway for financial support and computing time at the Norwegian supercomputer facilities.

*Corresponding author: ravindran.vidya@kjemi.uio.no

[1] T. Minami, Thin Solid Films **516**, 5822 (2008).
[2] T. Yoshida, M. Tochimoto, D. Schlettwein, D. Wöhrle, T. Sugiura, and H. Minoura, Chem. Mater. **11**, 2657 (1999).
[3] K. Moritomo, in *Phosphor Handbook*, edited by S. Shionoya and W. M. Ren (CRC Press, Cleveland, OH, 1999), p. 561.
[4] D. C. Look, Mater. Sci. Eng. **80**, 383 (2001).
[5] D. C. Look, J. Electron. Mater. **35**, 1299 (2006).
[6] A. E. Rakhshani, J. Kokaj, J. Mathew, and B. Peradeep, Appl. Phys. A **86**, 377 (2007).
[7] S. F. Chichibu, T. Onuma, M. Kubota, A. Uedono, T. Sota, A. Tsukazaki, A. Ohtomo, and M. Kawasaki, J. Appl. Phys. **99**, 093505 (2006).
[8] Y. G. Wang, S. P. Lau, X. H. Zhang, H. W. Lee, S. F. Yu, B. K. Tay, and H. H. Hng, Chem. Phys. Lett. **375**, 113 (2003).
[9] A. F. Kohan, G. Ceder, D. Morgan, and C. G. Van de Walle, Phys. Rev. B **61**, 15019 (2000).
[10] F. Oba, S. R. Nishitani, S. Isotani, H. Adachi, and I. Tanaka, J. Appl. Phys. **90**, 824 (2001).
[11] S. B. Zhang, S.-H. Wei, and A. Zunger, Phys. Rev. B **63**, 075205 (2001).
[12] S. Lany and A. Zunger, Phys. Rev. B **72**, 035215 (2005).
[13] C. Persson, Y.-J. Zhao, S. Lany, and A. Zunger, Phys. Rev. B **72**, 035211 (2005).
[14] A. Janotti and C. G. Van de Walle, J. Cryst. Growth **287**, 58 (2005).
[15] A. Janotti and C. G. Van de Walle, Appl. Phys. Lett. **87**, 122102 (2005).
[16] P. Erhart and K. Albe, Appl. Phys. Lett. **88**, 201918 (2006).
[17] P. Erhart, K. Albe, and A. Klein, Phys. Rev. B **73**, 205203 (2006).
[18] A. Janotti and C. G. Van de Walle, Phys. Rev. B **76**, 165202 (2007).
[19] S. Lany and A. Zunger, Phys. Rev. Lett. **98**, 045501 (2007).
[20] T. R. Paudel and W. R. L. Lambrecht, Phys. Rev. B **77**, 205202 (2008).
[21] F. Oba, A. Togo, I. Tanaka, J. Paier, and G. Kresse, Phys. Rev. B **77**, 245202 (2008).
[22] P. Agoston, K. Albe, R. M. Nieminen, and M. J. Puska, Phys. Rev. Lett. **103**, 245501 (2009).
[23] S. Lany and A. Zunger, Phys. Rev. B **78**, 235104 (2008).
[24] C. W. M. Castleton, A. Höglund, and S. Mirbt, Model. Simul. Mater. Sci. Eng. **17**, 084003 (2009).
[25] P. E. Blöchl, Phys. Rev. B **50**, 17953 (1994).
[26] G. Kresse and J. Furthmuller, Comput. Mater. Sci. **6**, 15 (1996).
[27] J. P. Perdew, K. Burke, and M. Ernzerhof, Phys. Rev. Lett. **77**, 3865 (1996).
[28] D. R. Lide, ed. *Handbook of Chemistry and Physics*, 85th ed. (CRC Press, Boca Raton, FL, 2004).
[29] A. Every and A. McCurdy, *Landolt-Bornstein: Numerical Data and Functional Relationships in Science and Technology, New Series* (Springer, Heidelberg, 1992), Vol. III/29A.
[30] K. P. Huber and G. Herzberg, *Constants of Diatomic Molecules* (Van Nostrand, New York, 1979).
[31] P. M. Mooney, in *Identification of Defects in Semiconductors, and Semimetals*, edited by M. Stavola (Academic Press, San Diego, CA, 1999), Vol. 51B, p. 93.
[32] K. Laaksonen, M. G. Ganchenkova, and R. M. Nieminen, J. Phys. Condens. Matter **21**, 015803 (2009).
[33] G. Makov and M. C. Payne, Phys. Rev. B **51**, 4014 (1995).
[34] S. B. Zhang, S.-H. Wei, A. Zunger, and H. Katayama-Yoshida, Phys. Rev. B **57**, 9642 (1998).
[35] S. Zh. Karazhanov, P. Ravindran, A. Kjekshus, H. Fjellvåg, U. Grossner, and B. G. Svensson, J. Appl. Phys. **100**, 043709 (2006).
[36] C. J. Vesely, R. L. Hengehold, and D. W. Langer, Phys. Rev. B **5**, 2296 (1972).
[37] L. Ley, R. A. Pollak, F. R. McFeely, S. P. Kowalczyk, and D. A. Shirley, Phys. Rev. B **9**, 600 (1974).
[38] C. Klingshirn, Phys. Status Solidi B **244**, 3027 (2007).
[39] M. G. Ganchenkova and R. M. Nieminen, Phys. Rev. Lett. **96**, 196402 (2006).
[40] D. C. Look, D. C. Reynolds, J. R. Sizelove, R. L. Jones, C. W. Litton, G. Cantwell, and W. C. Harsch, Solid State Commun. **105**, 399 (1998).
[41] C. H. Seager and S. M. Myers, J. Appl. Phys. **94**, 2888 (2003).
[42] U. Grossner, S. Gabrielsen, T. M. Børseth, J. Grillenberger, A. Yu. Kuznetsov, and B. G. Svensson, Appl. Phys. Lett. **85**, 2259 (2004).
[43] H. von Wenckstern, H. Schmidt, M. Grundmann, M. W. Allen, P. Miller, R. J. Reeves, and S. M. Durbin, Appl. Phys. Lett. **92**, 022913 (2007).
[44] J. F. Cordaro, Y. Shim, and J. E. May, J. Appl. Phys. **60**, 4186 (1986).
[45] H. Morkoc and U. Ozgur, *Zinc Oxide: Fundamentals, Materials and Device Technology* (Wiley-VCH Verlag, Weinheim, 2009), p. 180.
[46] J. Neugebauer and C. G. Van de Walle, Appl. Phys. Lett. **69**, 503 (1996).
[47] S. Lany and A. Zunger, Phys. Rev. Lett. **93**, 156404 (2004).
[48] A. A. Sokol, S. A. French, S. T. Bromley, R. A. Catlow, H. J. J. van Dam, and P. Sherwood, Faraday Discuss. **134**, 267 (2007).
[49] C. G. Van de Walle and J. Neugebauer, J. Appl. Phys. **95**, 3851 (2004).
[50] M. Mikami, T. Eto, J. Wang, Y. Masa, and M. Isshiki, J. Cryst. Growth **276**, 389 (2005).
[51] M. Mikami, S.-H. Hong, T. Sato, S. Abe, J. Wang, K. Masumoto, Y. Masa, and M. Isshiki, J. Cryst. Growth **304**, 37 (2007).
[52] M. A. Reshchikov, S. Nagata, J. Xie, B. Hertog, and A. Osinsky, Mater. Res. Soc. Symp. Proc. **1035**, L13-12 (2008).
[53] M. A. Reshchikov and H. Morko, J. Appl. Phys. **97**, 061301 (2005).
[54] M. A. Reshchikov, J. Q. Xie, B. Hertog, and A. Osinsky, J. Appl. Phys. **103**, 103514 (2008).
[55] T. Moe Børseth, B. G. Svensson, and A. Yu. Kuznetsov, P. Klason, Q. X. Zhao, and M. Willander, Appl. Phys. Lett. **89**, 262112 (2006).
[56] S. A. Studenikin, N. Golego, and M. Cocivera, J. Appl. Phys. **84**, 5001 (1998).
[57] S. Y. Myong and K. S. Lim, J. Cryst. Growth **293**, 253 (2006).
[58] S.A. Studenikin and M. Cocivera, J. Appl. Phys. **91**, 5060 (2002).
[59] Y. W. Heo, D. P. Norton, and S. J. Pearton, J. Appl. Phys. **98**, 073502 (2005).
[60] Y. J. Lin, C.-L. Tsai, Y.-M. Lu, and C.-J. Liu, J. Appl. Phys. **99**, 093501 (2006).
[61] P. Cheng, S. Li, L. Zhang, and J. Li, Appl. Phys. Lett. **93**, 012902 (2008).
[62] Y.-S. Kim and C. H. Park, Phys. Rev. Lett. **102**, 086403 (2009).
[63] C. D. Pemmaraju, R. Hanafin, T. Archer, H. B. Braun, and S. Sanvito, Phys. Rev. B **78**, 054428 (2008).
[64] L. S. Vlasenko and G. D. Watkins, Phys. Rev. B **71**, 125210 (2005).

[65]F. Tuomisto, K. Saarinen, D. C. Look, and G. C. Farlow, Phys. Rev. B **72**, 085206 (2005).

[66]A. Savin, R. Nesper, S. Wengert, and T. F. Fssler, Angew. Chem. Int. Ed. Engl. **36**, 1808 (1997).

[67]P. Blaha, K. Schwarz, G. K. H. Madsen, D. Kvasnicka, and J. Luitz, WIEN2k, *An Augmented Plane Waves + Local Orbitals Program for Calculating Crystal Properties*, rev. ed. (Vienna University of Technology, Vienna, 2008).

[68]R. Vidya, P. Ravindran, K. Knizek, A. Kjekshus, and H. Fjellvåg, Inorg. Chem. **47**, 6608 (2008).

[69]J. D. Ye, S. L. Gu, F. Li, S. M. Zhu, R. Zhang, Y. Shi, Y. D. Zheng, X. W. Sun, and G. Q. Lo, and D. L. Kwong, Appl. Phys. Lett. **90**, 152108 (2007).

[70]P. S. Xu, Y. M. Sun, C. S. Shi, F. Q. Xu, and H. B. Pan, Nucl. Instrum. Methods Phys. Res. Sect. B **199**, 286 (2003).